Kinetic Study of Fischer Tropsch Synthesis over co Precipitated Iron-Cerium Catalyst

A.A. Mirzaei[a,*], M. Arsalanfar[a], F. Ebrahimzadeh[a], H. Atashi[b] and S.H. Mirhoseini Moghaddam[c]

[a]*Department of Chemistry, Faculty of Sciences, University of Sistan and Baluchestan, Zahedan 98135-674*
[b]*Department of Chemical Engineering, Faculty of Engineering,*
University of Sistan and Baluchestan, P.O. Box 98164-161, Zahedan, Iran
[c]*Iran Polymer and Petrochemical Institute, P.O. Box 14965/115, Tehran, Iran*

The kinetic of Fischer-Tropsch synthesis over a co-precipitated Fe-Ce catalyst was investigated in a fixed bed micro reactor. Experimental conditions were varied as follow: reaction pressure 1-15 bar, H_2/CO feed ratio of 1-3 and space velocity of 3600-5400 h^{-1} at the temperature range of 270-310 °C. Four models according to the Langmuir-Hinshelwood-Hougen-Watson (LHHW) type rate equation were derived on the basis of detailed set of possible reaction mechanisms. The reaction rate of this study is fitted fairly well by one kinetic expression based on LHHW mechanism. The kinetic parameters were estimated *via* non-linear regression method and the MARR% values for all proposed models were obtained. The activation energy was 72 kJ mol^{-1} for optimum kinetic model. This model had the lower MARR% value than those of the other proposed models.

INTRODUCTION

The Fischer-Tropsch synthesis (FTS) in which syngas is converted into a wide product spectrum consisting of a complex multi-component mixture of linear and branched hydrocarbons and oxygenates, has been found renewed interest particularly in the context of the indirect conversion of coal or natural gas to liquid transportation fuels. Synthesis gas can be obtained from any carbonaceous material, preferentially containing hydrogen [1]. Coal and natural gas are the most common sources to produce synthesis gas. Advantages of the FT hydrocarbons compared to crude oil derivatives are, *e.g.*, the absence of sulfur, nitrogen, and the low aromatic content [2]. From the viewpoint of economic viability, the selectivity considerations are extremely important in the design of FTS processes. To achieve an optimum in performance for the complete process, the catalyst and the reactor should be optimum comprehensively. It requires hierarchically the development of an engineering kinetics model, in which detailed product distribution information of FTS can self-consistently be reflected. The

quality of a detailed kinetic model is closely related to the understanding of the mechanism in the FTS catalytic reaction system, in which a polymerization process has been recognized to be dominant; however, sufficient details on the FTS mechanistic aspect are not yet fully understood [3-5]. In 1946, Herington first treated the molar distribution of hydrocarbons from FTS in terms of a polymerization mechanism [5,6]. The same formulation was rediscovered by Anderson *et al.* in 1951 and named the ASF distribution [6]. Investigating the kinetics of FT is important not only for optimizing process parameters, but also for shedding light on the catalytic mechanism [7,8]. In kinetic studies for developing of the CO consumption rate expressions, the hydrocarbon production information is always high significant [9-11]. The kinetic description of the FT reaction is very important task for the industrial practice, being a prerequisite for the industrial process design, optimization and simulation [12]. Iron-based catalysts provide both CO hydrogenation (FTS) and water-gas-shift (WGS) reaction activities, and allow the direct processing of synthesis gas with a low H_2/CO ratio (as produced by coal gasification in advanced gasifiers) without an additional WGS reactor [13]. The kinetics of FTS and WGS reactions over the iron-based catalyst were

---

*Corresponding author. E-mail: mirzaei@hamoon.usb.ac.ir

investigated by many researchers [14-17]. It is generally accepted that FTS and WGS reactions take place on different active sites over a precipitated iron catalyst and the two reactions will only influence each other *via* gas phase [15].

The main objectives of the present work are the investigation of the kinetic and mechanism of the CO hydrogenation on the co-precipitated Fe-Ce catalyst and also determining the kinetic parameters.

EXPERIMENTAL

Preparation

In this study the iron cerium catalyst was prepared using co-precipitation method as follows. Aqueous solutions $Ce(NO_3)_2.6H_2O$ (1 M) and $Fe(NO_3)_3.9H_2O$ (1 M) with molar ratio of [Fe]/[Ce] = 4/1 were pre-mixed and the resulting solution heated to 70 °C in a round-bottomed flask fitted with a condenser. Aqueous Na_2CO_3 (1 M) was added dropwise to the mixed nitrate solution with stirring while the temperature was maintained at 70 °C until pH = 8.3 ± 0.1 was achieved. The resulting precipitate was then left in this medium for 2 h. The aged suspension was then filtered, washed several times with warm distilled water until no further Na^+ was observed in the washings [18], as tested by flame atomic absorption. The precipitate was then dried in an oven at 110 °C for 16 h to give a material denoted as the catalyst precursor, which was subsequently calcined in static air in the furnace at 650 °C for 6 h to give the final catalyst.

Catalyst Testing

The catalyst tests were carried out in a fixed bed micro reactor operating at atmospheric pressure (Fig. 1). All gas lines to the reactor bed were made from 1/4" stainless steel tubing. Three mass flow controllers (Brooks, Model 5850E) equipped with a four-channel read out and control equipment (Brooks 0154) were used to adjust automatically the flow rate of the inlet gases (CO, H_2 and N_2 with purity of 99.999%). The mixed gases in the mixing chamber passed into the reactor tube, which was placed inside a tubular furnace (Atbin, Model ATU 150-15) capable of producing temperature up to 1500 ºC and controlled by a digital programmable controller (DPC). The reactor tube was constructed from stainless steel tubing; internal diameter of 20 mm, with the catalyst bed situated in
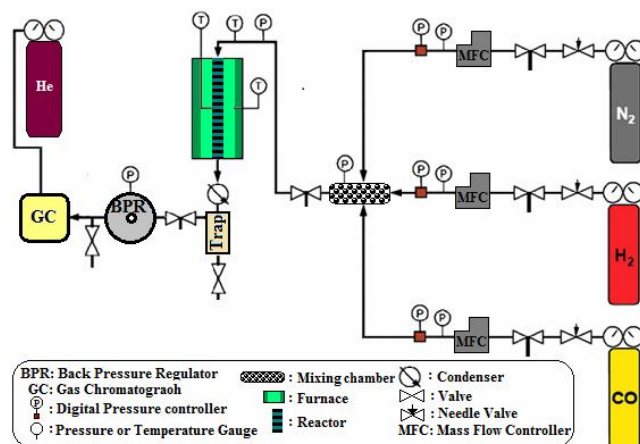
Fig. 1. Schematic representation of the reactor in a flow diagram used.

the middle of the reactor. The reaction temperature was controlled by a thermocouple inserted into catalyst bed and visually monitored by a computer equipped with software. Some thermocouples inserted in the catalyst bed for monitoring the inlet, outlet and bed temperatures by a DPC. The meshed catalyst (1.0 g) was held in middle of the reactor using quartz wool. It consist of an electronic back pressure regulator which can control the total pressure of the desired process using a remote control *via* the TESCOM software package integration that improve or modify its efficiency that capable for working on pressure ranging from atmospheric pressure to 100 bar. The catalyst was *in situ* pre-reduced at atmospheric pressure under H_2-N_2 (flow rate of each gas = 30 ml min^{-1}) at 400 ºC for 12 h before synthesis gas exposure. The FTS was carried out under in the range of 270-310 °C, P = 1-15 bar, H_2/CO = 1/1-3/1 and GHSV = 3600-5400 h^{-1}. In each test, 1.0 g catalyst was loaded and the reactor operated about 12 h to ensure steady state operations were attained. Reactant and product streams were analyzed on-line using a gas chromatograph (Thermo ONIX UNICAM PROGC+) equipped with sample loop, two Thermal Conductivity Detector (TCD) and one Flame Ionization Detector (FID) able to perform the analysis of a wide variety of gaseous hydrocarbon mixtures, one TCD used for the analysis of hydrogen and the other one used for all the permanent gases such as N_2, O_2 and CO. The FID is used for the analysis of hydrocarbons. The contents of the sample loop were injected

70

automatically into an alumina capillary column (30 m × 0.550 mm). Helium was employed as a carrier gas for optimum sensitivity (flow rate = 30 ml min^{-1}). The GC calibration was carried out using various calibration mixtures and pure compounds obtained from American Matheson Gas Company (USA). The results in terms of CO conversion and selectivity of products are given at each space velocity. The CO conversion (%) is calculated according to the normalization method:

$$CO\,conversion\,(\%) = \frac{(Moles\,of\,CO_{in}) - (Moles\,of\,CO_{out})}{(Moles\,of\,CO_{in})} \times 100 \tag{1}$$

The selectivity (%) towards the individual components on carbon-basis is calculated according to the same principle:

$$Selectivity\,of\,j\,product\,(\%) = \frac{Moles\,of\,carbon\,in\,product\,j}{Moles\,of\,converted\,CO} \times 100 \tag{2}$$

RESULTS AND DISCUSSION

Reactor Model

An integral reactor model was used to describe the operation of the micro fixed bed reactor. The heat transfer in this reactor was also such that the catalyst packing was essentially isothermal for the operating conditions used. The effects of axial dispersion and pressure drop were examined with well-established criteria [19,20] and it was found that all of these effects can be neglected. It was accordingly deduced that an isothermal one-dimensional pseudo homogeneous model with plug flow was applicable. The equations describing this model consist of a mass balance for each particular component which may be written as flows:

$$\frac{d(uC_i)}{dZ} + r_i\rho_\beta = 0 \tag{3}$$

Where C_i refers to the concentration of component i (mol m^{-3}), u the superficial velocity (m s^{-1}), r_i the overall reaction rate of component i [mol kg$_{cat}^{-1}$ s^{-1})], and ρ_β the catalyst bed density (kg$_{cat}$ m^{-3}). With the boundary condition $C_i = C_i^\circ$ at reactor entrance (Z = 0), the overall synthesis reaction can be written

as follows:

$$nCO + (n + m/2)H_2 \rightarrow C_nH_m + nH_2O \tag{4}$$
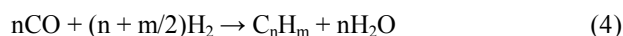
where n is the average carbon chain length of the hydrocarbon product and m is the average number hydrogen atoms per hydrocarbon molecule [21].

Experimental Results

Experiments were carried out with mixtures of H$_2$, CO and N$_2$ in a temperature range of 270-310 °C, H$_2$/CO feed ratio of 1/1-3/1 and a pressure range of 1-15 bar. The experimental conditions and obtained data are presented in Table 1. To avoid the effect of deactivation, fresh catalysts were loaded in each experiment series. To achieve the isothermal conditions in a catalytic bed, the catalyst was diluted with inert materials (quartz and asbestos), axial temperature distribution was ensured using Mear's criterion [22,23]. To avoid of channelization phenomena, the following simplified relation between catalyst bed length (L$_b$) and mean catalyst particle diameter (d$_p$) was fulfilled, L$_b$/dp > 50. We have a differential flow reactor when we choose to consider the rate to be constant at all points within the reactor. Since rates are concentration-dependent this assumption is usually reasonable only for small conversions or for shallow small reactors. For each run in a differential reactor, the plug flow performance equation becomes as follows:

$$\frac{W}{F_{CO}^\circ} = \int_{x_{in}}^{x_{out}} \frac{d_x}{-r_A'} = \frac{-1}{r_A'}\int_{x_{in}}^{x_{out}} dx = \frac{x_{out} - x_{in}}{-r_A'} = \frac{x_{out} - 0}{-r_A'} \tag{5}$$

According to the above equation, the average rate for each run is derived as follow:

$$-r_A' = \frac{F_{CO}^\circ x_{out}}{W} \tag{6}$$

The CO conversion and percentages of product selectivities, present in steady state catalytic performance are presented in Table 2. As seen, at different operational conditions the CO conversion and selectivities toward different products have been changed.

Kinetic Modeling and Reaction Rate Equations

To obtain the rate equation, a reaction mechanism should

71

Table 1. Summary of Experimental Conditions and Results for Kinetic Tests at P_{tot} = 1-15 bar, T = 270-310 °C and H_2/CO = 1/1-3/1 in a Fixed Bed Reactor (FBR)

No.	T (K)	P (bar)	H_2/CO ratio	P_{CO} (bar)	P_{H2} (bar)	X_{CO} (%)	$R_{CO} \times 10^{+4}$ (mmol min^{-1} g$_{cat}^{-1}$)
1	583.15	1	1.0	0.40	0.40	4.25	10.5128
2	583.15	1	1.5	0.27	0.40	13.84	15.2286
3	573.15	1	1.5	0.27	0.40	6.07	6.78999
4	563.15	1	1.5	0.27	0.40	2.96	3.36931
5	553.15	1	1.5	0.27	0.40	12.01	13.9338
6	543.15	1	1.5	0.27	0.40	10.61	12.5456
7	543.15	1	2.0	0.27	0.53	11.49	13.5825
8	553.15	1	2.0	0.27	0.53	14.26	16.5436
9	563.15	1	2.0	0.27	0.53	12.54	14.2901
10	583.15	1	2.0	0.27	0.53	10.99	12.1029
11	583.15	1	2.5	0.21	0.53	18.26	12.8637
12	543.15	1	3.0	0.20	0.60	10.75	7.14393
13	553.15	1	3.0	0.20	0.60	11.13	7.26463
14	563.15	2	1.0	0.80	0.80	3.49	179.174
15	553.15	2	1.0	0.80	0.80	5.92	100.457
16	543.15	2	1.5	0.53	0.80	7.84	18.5155
17	553.15	2	1.5	0.53	0.80	11.80	27.3960
18	563.15	2	1.5	0.53	0.80	12.25	27.9125
19	573.15	2	1.5	0.53	0.80	14.99	33.5645
20	583.15	2	1.5	0.53	0.80	22.20	48.8710
21	583.15	2	2.0	0.53	1.07	6.12	57.4850

Table 2. The Catalytic Performance of the Fe-Ce Catalyst under Operational Conditions

T (K)	H_2/CO	Selectivity (%)					
		CH_4	C_2H_6	C_2H_4	C_3H_8	C_3H_6	C_4^+
583.15	1.0	59.98	9.21	15.50	7.19	5.08	3.02
583.15	1.5	61.02	3.29	17.82	5.08	8.12	4.65
573.15	1.5	57.45	1.65	22.43	3.35	13.36	1.73
563.15	1.5	46.35	1.33	22.09	6.75	20.21	3.25
553.15	1.5	47.64	12.06	13.07	7.50	17.10	2.61
543.15	1.5	44.28	2.54	23.61	1.23	23.37	4.93
543.15	2.0	40.77	2.39	25.24	1.38	25.30	4.90
553.15	2.0	37.80	3.37	26.36	1.52	28.62	2.30
563.15	2.0	36.65	4.64	26.12	1.72	28.97	1.87
583.15	2.0	39.84	8.38	22.87	4.45	23.18	1.29
583.15	2.5	40.83	4.91	27.03	1.45	24.88	0.88
543.15	3.0	43.74	4.75	27.13	1.29	22.18	0.88
553.15	3.0	48.39	13.20	17.27	6.32	14.14	0.65
563.15	1.0	48.44	3.57	27.72	0.90	18.65	0.69
553.15	1.0	49.28	3.31	27.80	0.83	18.26	0.48
543.15	1.5	50.11	3.27	27.53	0.79	17.73	0.54
553.15	1.5	50.95	3.50	26.85	0.82	17.33	0.51
563.15	1.5	52.28	3.90	25.77	0.88	16.74	0.40
573.15	1.5	55.01	4.42	24.19	0.93	15.08	0.35
583.15	1.5	56.95	5.58	21.94	1.07	14.12	0.31
583.15	2.0	62.74	7.69	16.08	1.53	11.66	0.26

72

be adopted. For determination of kinetic model, four mechanisms were offered on the basis of various monomer formation (elementary reactions) and carbon chain distribution pathways. An elementary reaction set on sites for each model is summarized in Table 3. To derivation of each kinetic model, initially one of the elementary reaction steps was assumed as rate determination step and all other steps were considered at equilibrium. Then, all of the obtained models were fitted separately, against experimental data. Table 4 displays the final form of different rate expressions for the 4 kinetic models. The development of the kinetic equations will be illustrated for FT-III2 model (the second step of the elementary reaction for the FT-III model). The model codes refer to the set of elementary reactions and the elementary reaction is not at equilibrium (that is the rate-determining step, so in this case reaction 2). The set of elementary reactions for FT-III2 model is shown in Table 3. The reaction rate of the rate-determining step is:

$$-R_{CO} = k_2\theta_{CO}.P_{H2}(mol_{CO}.g_{cat}^{-1}.\min^{-1}) \tag{7}$$

where θ_{CO} is the surface fraction occupied with the associative absorbed carbon monoxide. The surface fractions of carbon monoxide can be calculated from the site balance, the preceding reaction steps which are at quasi-equilibrium:

$$\theta_S + \theta_{CO} = 1 \tag{8}$$

$$K_1 = \frac{k_1}{k_{-1}} = \frac{\theta_{CO}}{P_{CO}\theta_S} \Rightarrow \theta_{CO} = K_1 P_{CO}\theta_S \tag{9}$$

Substituting Eq. (9) into Eq. (8), the concentration of free active site can be expressed as:

$$\theta_S + \theta_{CO} = 1 \Rightarrow \theta_S + K_1.P_{CO}.\theta_S = 1 \Rightarrow \theta_S = \frac{1}{1 + K_1.P_{CO}} \tag{10}$$

By substituting of Eq. (10) into Eq. (9), the expression of θ_{CO} becomes:

$$\theta_{CO} = \frac{K_1.P_{CO}}{1 + K_1.P_{CO}} \tag{11}$$

With substituting the surface fraction of CO (Eq. (11)) in Eq.

Table 3. Reaction Schemes of FTS

Model	No.	Elementary reaction
	1	$CO + 2s \leftrightarrow Cs + Os$
	2	$H_2 + 2s \leftrightarrow 2Hs$
FT-I	3	$Cs + Hs \leftrightarrow HCs + s$
	4	$HCs + Hs \leftrightarrow H_2Cs + s$
	5	$Os + Hs \rightarrow HOs + s$
	6	$HOs + Hs \rightarrow H_2O + 2s$
	1	$CO + s \leftrightarrow COs$
	2	$H_2 + 2s \leftrightarrow 2Hs$
	3	$COs + Hs \leftrightarrow HCOs + s$
	4	$HCOs + H_s \leftrightarrow Cs + H_2O +$
FT-II	5	s
	6	$Cs + H_s \leftrightarrow CHs + s$
	7	$CHs + H_s \leftrightarrow CH_2s + s$
	8	$O_s + H_s \rightarrow HO_s + s$
		$HO_s + H_s \rightarrow H_2O + 2s$
	1	$CO + s \leftrightarrow COs$
FT-III	2	$COs + H_2 \leftrightarrow H_2COs$
	3	$H_2COs + H_2 \leftrightarrow CH_2s + H_2O$
	1	$CO + s \leftrightarrow Cos$
	2	$H_2 + s \leftrightarrow H_2s$
FT-IV	3	$Cos + H_2s \leftrightarrow H_2Cos + s$
	4	
		$H_2Cos + H_2s \leftrightarrow H_2O + s$

(7), the final rate expression is obtained:

$$-R_{CO} = \frac{KP_{CO}P_{H_2}}{1 + aP_{CO}} \tag{12}$$

which K and a parameters are defined as follow:

$$K = k_2 K_1 \text{ and } \alpha = K_1$$

73

Table 4. Reaction Rate Expressions for the FTS

| Number of proposed model	Rate equation	Parameters	MARR (%)
FT-I-1	$-R_{CO} = \dfrac{K.P_{CO}}{[1 + 2(\alpha P_{CO})^{0.5} + (\beta P_{H2})^{0.5}]^2}$	$K = k_1$ $\alpha = \dfrac{k_1}{k_{-1}}$ $\beta = \dfrac{k_2}{k_{-2}}$	15.21
FT-I-2	$-R_{CO} = \dfrac{K.P_{H2}}{[1 + 2(\alpha P_{CO})^{0.5} + (\beta P_{H2})^{0.5}]^2}$	$K = k_1$ $\alpha = \dfrac{k_1}{k_{-1}}$ $\beta = \dfrac{k_2}{k_{-2}}$	17.32
FT-I-3	$-R_{CO} = \dfrac{K.P_{CO}^{0.5}.P_{H2}^{0.5}}{[1 + 2(\alpha P_{CO})^{0.5} + (\beta P_{H2})^{0.5}]^2}$	$K = k_3.K_1^{0.5}.K_2^{0.5}$ $\alpha = \dfrac{k_1}{k_{-1}}$ $\beta = \dfrac{k_2}{k_{-2}}$	19.45
FT-I-4	$-R_{CO} = \dfrac{K.P_{CO}^{0.5}.P_{H2}}{[1 + 2(\alpha P_{CO})^{0.5} + (\beta P_{H2})^{0.5}]^2}$	$K = k_4.K_3.K_2.K_1^{0.5}$ $\alpha = \dfrac{k_1}{k_{-1}}$ $\beta = \dfrac{k_2}{k_{-2}}$	21.62
FT-II-1	$-R_{CO} = \dfrac{K..P_{CO}}{1 + \alpha P_{CO} + (\beta P_{H2})^{0.5}}$	$K = k_1$ $\alpha = \dfrac{k_1}{k_{-1}}$ $\beta = \dfrac{k_2}{k_{-2}}$	13.49
FT-II-2	$-R_{CO} = \dfrac{K.P_{H2}}{1 + \alpha P_{CO} + (\beta P_{H2})^{0.5}}$	$K = k_1$ $\alpha = \dfrac{k_1}{k_{-1}}$ $\beta = \dfrac{k_2}{k_{-2}}$	22.75
FT-II-3	$-R_{CO} = \dfrac{K.P_{CO}.P_{H2}^{0.5}}{[1 + \alpha P_{CO} + (\beta P_{H2})^{0.5}]^2}$	$K = k_3.K_1.K_2$ $\alpha = \dfrac{k_1}{k_{-1}}$ $\beta = \dfrac{k_2}{k_{-2}}$	24.63
FT-II-4	$-R_{CO} = \dfrac{K.P_{CO}.P_{H2}}{[1 + \alpha P_{CO} + (\beta P_{H2})^{0.5}]^2}$	$K = k_4.K_2.K_3.K_4$ $\alpha = \dfrac{k_1}{k_{-1}}$ $\beta = \dfrac{k_2}{k_{-2}}$	19.53
FT-III-1	$-R_{CO} = \dfrac{K.P_{CO}}{1 + \alpha P_{CO}}$	$K = k_1$ $\alpha = \dfrac{k_1}{k_{-1}}$	27.41
FT-III-2	$-R_{CO} = \dfrac{K.P_{CO}.P_{H2}}{1 + \alpha P_{CO}}$	$K = k_2.K_1$ $\alpha = \dfrac{k_1}{k_{-1}}$	12.14
FT-III-3	$-R_{CO} = \dfrac{K.P_{CO}.P_{H2}^2}{1 + \alpha P_{CO}}$	$K = k_3.K_1.K_2$ $\alpha = \dfrac{k_1}{k_{-1}}$	25.41
FT-IV-1	$-R_{CO} = \dfrac{K.P_{CO}}{1 + \alpha P_{CO} + \beta P_{H2}}$	$K = k_1$ $\alpha = \dfrac{k_1}{k_{-1}}$ $\beta = \dfrac{k_2}{k_{-2}}$	16.27
FT-IV-2	$-R_{CO} = \dfrac{K.P_{H2}}{1 + \alpha P_{CO} + \beta P_{H2}}$	$K = k_1$ $\alpha = \dfrac{k_1}{k_{-1}}$ $\beta = \dfrac{k_2}{k_{-2}}$	28.56
FT-IV-3	$-R_{CO} = \dfrac{K.P_{CO}.P_{H2}}{(1 + \alpha P_{CO} + \beta P_{H2})^2}$	$K = k_3.K_1.K_2$ $\alpha = \dfrac{k_1}{k_{-1}}$ $\beta = \dfrac{k_2}{k_{-2}}$	19.68

Parameters Optimization

Model parameters were calculated from the experimental data and optimized with statistical indicators. The various plots were provided by the Poly math software 6.0 to assess the quality of the regression models and compare the various models. The parameters used in the Poly math software 6.0 consist of graph, residual plot, confidence interval, R^2, R^2_{adj} Variance and R_{msd} which are defined as follows:

Graph. Graph is a plot, on the bases of the calculated and measured values of R_{CO} for each proposed model. An appropriate model shows different trends. Figure 2 compares the experimental and calculated R_{CO} for expression which was obtained for FT-III-2 (Table 3) with assumption that the step 2 is the rate controlling step.

Residual plot. The residual plot shows the difference between the calculated and measured values of the dependent variable as function of the measured values. The residuals between proposed model and experiment should be normally distributed with zero average line. A comparison between calculated and experimental CO conversion is presented in Fig. 3. This figure showed that the residual relative errors (RRs) between model and experiment are mostly distributed within zero line.

Confidence interval. If the confidence interval be smaller (or at least equal) than the respective parameter values (in absolute values), then the regression model is stable and statistically valid.

R^2 and R^2_{adj}. The correlation coefficients were used to
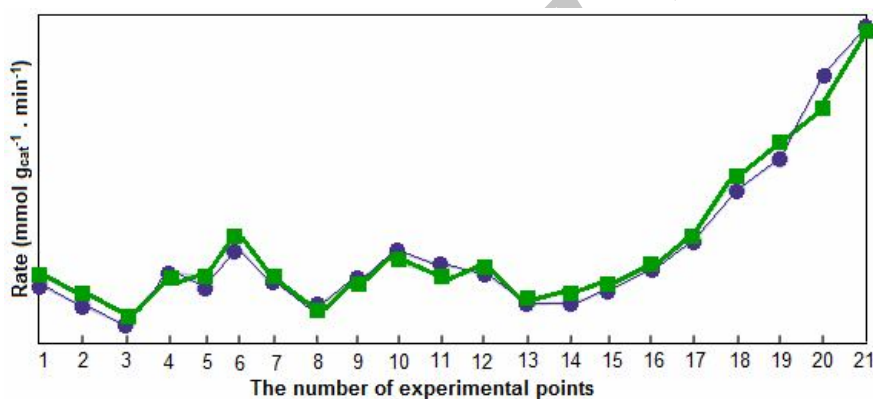
Fig. 2. Comparison between experimental and calculated reaction rate using equation 12. Reaction conditions: T = 270-310 °C, P = 1-15 bar, H_2/CO = 1/1-3/1 (o R_{exp} □ R_{cal}).
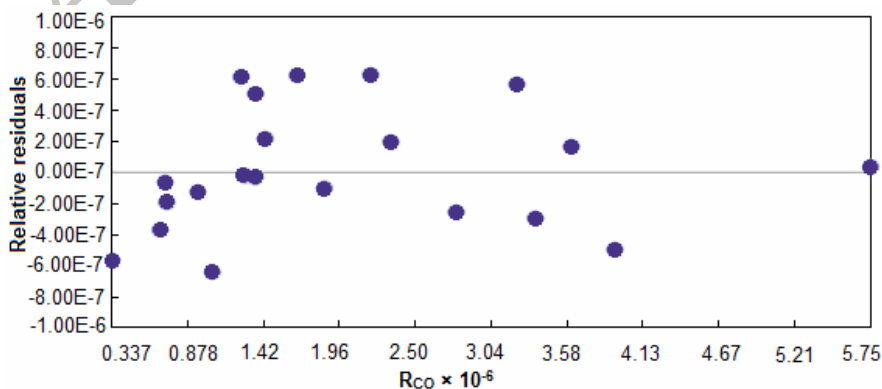
Fig. 3. The relative residuals for CO consumption rate (o R_{exp} - R_{cal}).

75

judge whether the model represents correctly the data. These parameters are defined as Eqs. (13-15).

$$\bar{y} = \frac{1}{n}(\sum_{i=1}^{n} yi_{\exp}) \tag{13}$$

$$R^2 = 1 - \frac{\sum_{i=1}^{n}(yi_{\exp} - yi_{calc})^2}{\sum_{i=1}^{n}(yi_{\exp} - \bar{y})} \tag{14}$$

$$R^2{}_{adj} = 1 - \frac{(1-R^2)(n-1)}{n-p} \tag{15}$$

In above formulas, the notations *n, y_i exp and calc* denote the number of experimental, specific observation, observed data and calculated data, respectively.

Variance and R_{msd}. Variance and R_{msd} are defined as Eqs. (16) and (17).

$$S^2 = \frac{\sum_{i=1}^{n}(y_i - \bar{y})^2}{(n-1)} \tag{16}$$

$$R_{msd} = \frac{1}{n}\left[\sum_{i=}^{n}(yi_{\exp} - yi_{calc})^2\right] \tag{17}$$

Some statically indicators used to assess the quality of the proposed model (expression FT-III, RDS.2), in Table 4, are summarized in Table 5.

Estimation of Kinetic Parameters

For estimation of the best kinetic model we assumed that:
1- Because of the small particle size of catalyst (180-250 µm), dilution of catalyst particles by asbestos and low CO conversion, the mass transport limitations and pressure drop can be neglected.

2- All parameters must be positive and all proposed models with negative parameters were rejected.

Parameters estimation and model discrimination have done by nonlinear regression model and using of the Poly math software 6.0. Figure 3 showed the residuals between proposed model and experimental data distributed randomly around zero line. Therefore, the proposed models were in good agreement with the experimental data.

We obtained the best expression that described the experimental results for FT reaction and it is as follow (Eq. (12)):

$$-R_{CO} = \frac{KP_{CO}P_{H_2}}{1+aP_{CO}}$$

Table 5. Values of Kinetic Parameters of FT-III-2 Model

Parameter	Value	Dimension
K_0	5.40×10^3	mmol g_{cat}^{-1} min^{-1} bar^{-1}
E_0	72.00	kJ mol^{-1}
$k_{(543.15)}$	6.49×10^4	mmol g_{cat}^{-1} min^{-1} bar^{-1}
$k_{(553.15)}$	8.42×10^4	mmol g_{cat}^{-1} min^{-1} bar^{-1}
$k_{(563.15)}$	1.09×10^4	mmol g_{cat}^{-1} min^{-1} bar^{-1}
$k_{(573.15)}$	1.53×10^4	mmol g_{cat}^{-1} min^{-1} bar^{-1}
$k_{(583.15)}$	1.98×10^4	mmol g_{cat}^{-1} min^{-1} bar^{-1}
a_0	8.30×10^{-8}	mmol g_{cat}^{-1} min^{-1} bar^{-1}
$H\Delta$	-47.00	kJ mol^{-1}
R^2	0.95	-
R_{msd}	1.01×10^{-7}	-
$R^2{}_{adj}$	0.93	-
Variance	2.26×10^{-13}	-
MARR (%)	12.14	-

76

The reaction rate of the FT reaction was evaluated over a range of temperature (523-573K), using Arrhenius-type equations (Eq. (18)) for the temperature dependence of the reaction rate constants.

$$K_i(T) = K_{i,0} \exp(-E_i) / RT \qquad (18)$$

$$a(T) = a_0 \exp(-\Delta H_{ads}) / RT \qquad (19)$$

where:

E_i: activation energy

ΔH_{ads} = adsorption enthalpy

by substituting Eqs. (18) and (19) in best fitted model (FT-III-2) we have:

$$-R_{CO} = \frac{(K_{i,0} \exp(-E_i)/RT)P_{CO}.P_{H2}}{(\alpha_0 \exp(-\Delta H_{ads})/RT)P_{CO}} \qquad (20)$$

The relation between the temperature and reaction rate constant is shown in Fig. 4. According to the Arrhenius-type equation (Eq. (18)), a plot of ln(k) *vs.* 1/T should give a straight line with negative slope of -E_i/R. The logarithm of the rate constant (k) which plotted in Fig. 4 as a function of reverse of temperature for catalyst shows this relationship between the temperature and rate constant. The relation between the temperature and adsorption enthalpy (Vanthouff plot) for the FT-III-2 model, is shown in Fig. 5.

The mean absolute relative residual (MARR%) between experimental and calculated consumption rate of CO is defined as:

$$MARR(\%) = \sum_{i=1}^{N_{exp}} \left| \frac{r_{exp} - r_{cal}}{r_{exp}} \right| \times \frac{1}{N_{exp}} \times 100 \qquad (21)$$

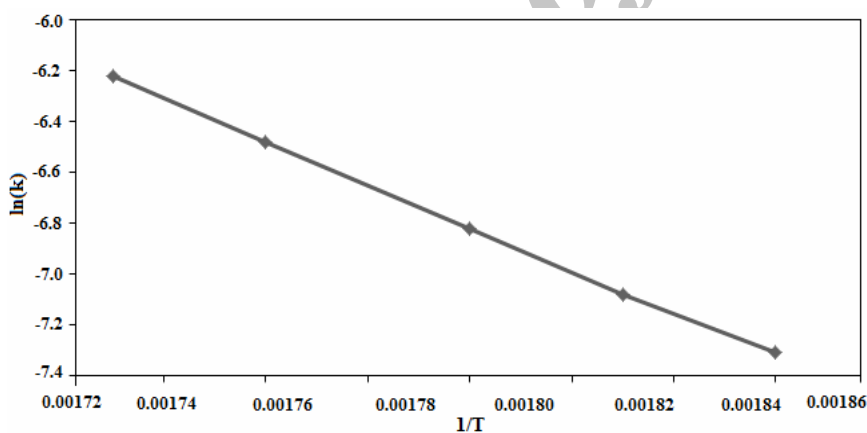where, N_{exp} is the number of data points included. Equation

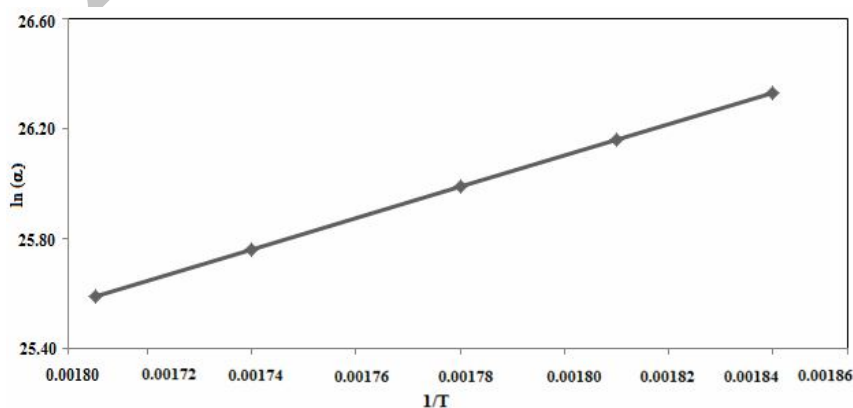**Fig. 4.** The Arhenius plot of rate constant (k).

Fig. 5. The Van't Hoff plot of (a) constant.

(12) shows the best fit to the experimental data. The comparison of the calculated and experimental consumption rate of CO for the FT-III-2 model is shown in Fig. 6 and the MARR% of this model was obtained 12.14%. This value is reasonable and shows that the predicted values are 12.14% different from the observed values. The MARR% values of the other obtained kinetic models are presented in Table 4; as shown the FT-III-2 model having the minimal MARR% value fits the experimental data well.

Catalyst Characterization

The XRD technique was carried out to identify the actual phases of Fe-Ce catalyst in different states of precursor and fresh calcined sample (the catalyst before the test). The XRD patterns of these samples are shown in Fig. 7. In the case of precursor, a high background in the low angle region reveals the presence of an amorphous phase in the different pattern due to indiscriminate scattering of X-rays. Consequently,

other phases that may be poorly crystalline or have small crystallite size, and hence broader peaks, are more difficult to detect. The actual phases identified in the calcined catalyst before the test, were Fe_2O_3 (rhombohedral) and Fe_3O_4 (cubic).

The XRD results showed that different carbonate and nitrate phases in the precursor state after calcination process were transformed to different oxidic phases of iron and cerium. In order to investigate the morphological features and changes in different states of precursor and fresh calcined samples (before the test) these samples were characterized using SEM method. The obtained electron micrographs presented in Fig. 8 show that the morphological features of the catalyst precursor and calcined samples are completely differed. The catalyst precursor is comprised of the particles with different sizes and undefined geometrical shapes; these particles have high dense agglomerate (Fig. 8a). After the calcination process the catalyst morphological feature is completely changed and this sample is comprised of the
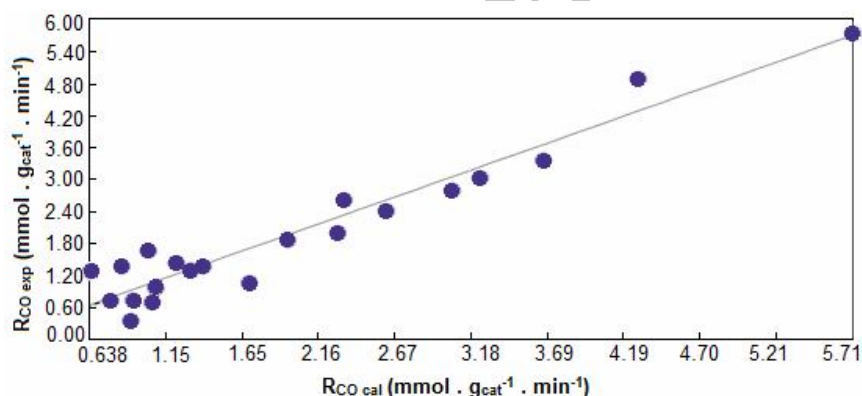

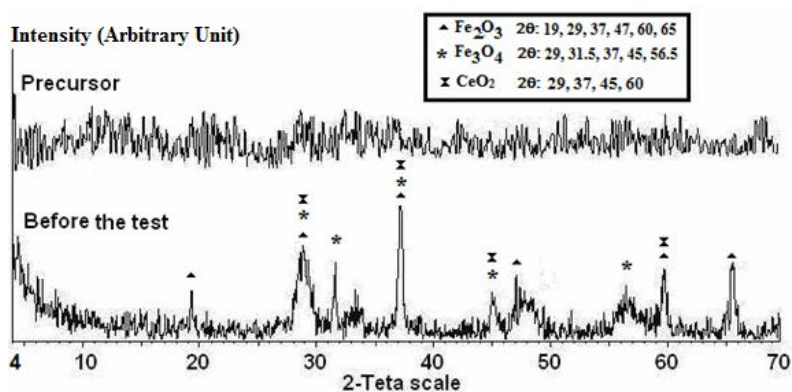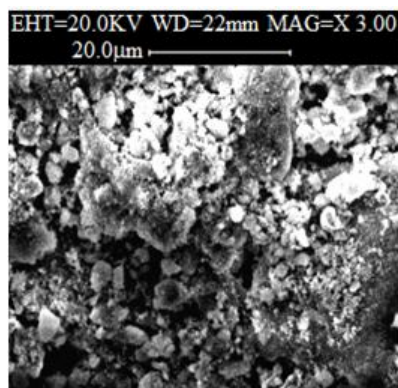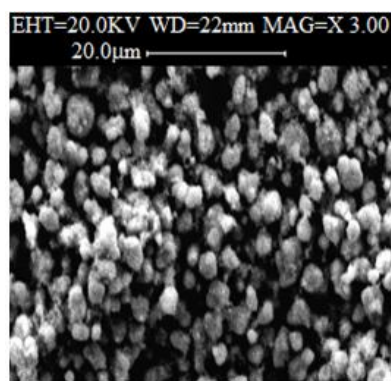**Fig. 6.** Thecomparison of calculated and experimental consumption rate of CO.

Fig. 7. XRD patterns of the Fe-Ce catalyst precursor and fresh calcined sample (▲ Fe_2O_3, * Fe_3O_4, ● CeO_2).

78

(a)

(b)

Fig. 8. The SEM images of the Fe-Ce catalyst in (a) precursor and (b) fresh calcined states.

spherical particles with the same sizes and has the lower particle agglomeration in compression with the precursor state (Fig. 8b).The SEM observation also confirmed that the calcinations process changed the morphological features of the catalyst.

CONCLUSIONS

The kinetic and mechanism of CO hydrogenation were investigated over the co-precipitated Fe-Ce catalyst in a fixed bed micro reactor. A number of Langmuir-Hinshelwood-Hougen-Watson type rate equations were derived on the basis of a detailed set of possible reaction mechanism. The unknown kinetic parameters were estimated from experimental data using linear regression method. The kinetic parameters

estimated the best fitted model (Eq. (12)), presented reasonable confidence intervals. The best fitted model (FT-III-2) shows that the rate-determining step proceeds *via* reaction associative adsorbed CO and H_2 molecule. The activation energy for the best fitted model was 72 kJ mol^{-1}; the logarithm of the rate constant (k) as a function of reveres of temperature showed a plot with negative slope of $-E_a/R$ and the rate equation of CO consumption was found as: $-R_{CO} = KP_{CO.} P_{H2}/1 + aP_{CO}$. The catalyst characterization was carried out using XRD and SEM techniques and the obtained results showed that characteristics of the catalyst are completely different in the cases of precursor and calcined sample.

REFERENCES

[1] M.E. Dry, A.P. Steynberg, Stud. Surf. Sci. Catal. 152 (2004) 406.

[2] M.E. Dry, Appl. Catal., A: Gen. 189 (1999) 185.

[3] A. Gribval-Constant, A.Y. Khodakov, R. Bechara, V.L. Zholobenko, Stud. Surf. Sci. Catal. 144 (2002) 609.

[4] V. Ponec, in H. Knoezinger, G. Ertl, J. Weitkamp (Eds.), Handbook of Heterogeneous Catalysis, VCH: Weinheim, Germany, Vol. 4, pp. 1879-1883.

[5] E.F.G. Herington, Chem. Ind. (London), 65 (1946) 346.

[6] R.A. Friedel, R.B. Anderson, J. Am. Chem. Soc. 72 (1950) 1212.

[7] W. Ma, G. Jacobs, D.E. Sparks, M.K. Gnanamani, V.R.R. Pendyala, C.H. Yen, J.L.S. Klettlinger, T.M. Tomsik, B.H. Davis, Fuel. 90 (2011) 756.

[8] M. Arsalanfar, A.A. Mirzaei, H. Atashi, H.R. Bozorgzade, S. Vahid, A. Zare, Fuel. Proc. Tech. 96 (2012) 150.

[9] M.J. Keyser, R.C. Everson, R.L. Espinoza, Ind. Eng. Chem. Res. 39 (2000) 48.

[10] G.P. Van der Laan, A.A.C.M. Beenackers, Appl. Catal. A: Gen. 193 (2000) 39.

[11] M.A. Vannice, J. Catal. 37 (1975) 462.

[12] H. Atashi, F. Siami, A.A. Mirzaei, M. Sarkari, J. Ind. & Eng. Chem. 16 (2010) 952.

[13] A. Nakhaei Pour, S.M.K. Shahri, Y. Zamani, M. Irani, S. Tehrani, J. Nat. Gas. Chem. 17 (2008) 242.

[14] B.-T. Teng, C.-H. Zhang, J. Yang, D.-B. Cao, J. Chang, H.-W. Xiang, Y.-W. Li, Fuel. 84 (2005) 719.

[15]   A. Nakhaei Pure, M.R. Housaindokht, S.F. Tayyari, J. Zarkesh, J. Natur. Gas. Chem. 19 (2010) 362.

[16]   Y.-N. Wang, W.-P. Ma, Y.-J. Lu, J. Yang, Y.-Y. Xu, H.-W. Xiang, Y.-W. Li, Y.-L. Zhao, B.-J. Zhang, Fuel. 82 (2003) 195.

[17]   B.-T. Teng, J. Chang, J. Yang, G. Wang, C.-H. Zhag, Y.-Y. Xu, H.-W. Xiang, Y.-W. Li, Fuel. 84 (2005) 917.

[18]   X. An, B. Wu, W. Hou, H. Wan, Z. Tao, T. Li, Z. Zhang, H. Xiang, Y. Li, B. Xu, F. Yi, J. Mol. Catal. A:

Chem. 263 (2007) 266.

[19]   R.C. Everson, H. Mulder, M.J. Keyser, Appl. Catal. A: Gen. 142 (1996) 223.

[20]   G.F. Forment, K.B. Bischoff, Chemical Reactor Analysis and Design, 2nd ed., Wiley, New York, 1990.

[21]   R.F. Blanks, Chem. Eng. Sci. 47 (1992) 959.

[22]   D.E. Mears**,** ACS Monogr. 133 (1974) 218.

[23]   M. Mollavali, F. Yaripour, H. Atashi, S. Sahebdelfar, Ind. Eng. Chem. Res. 47 (2008) 3265.

80